J Therm Anal Calorim (2012) 109:1245–1251
DOI 10.1007/s10973-012-2582-1

Inorganic reinforcement in PET/silica electrospun nanofibers

Qian Ma · Bin Mao · Peggy Cebe

Received: 31 October 2011 / Accepted: 29 June 2012 / Published online: 3 August 2012
© Akadémiai Kiadó, Budapest, Hungary 2012

Abstract PET/silica nanocomposite fibers of high quality were fabricated from electrospinning by choosing appropriate surface modification of inorganic fillers, solution properties, and processing conditions. The existence of an immobilized layer around silane-modified silica particles in PET fibers was verified by Fourier transform infrared spectroscopy, the results of which confirm previous thermal analysis studies. The influence of silica particles on the crystal growth during isothermal crystallization as well as the phase structure of the crystallized nanocomposite fibers were examined using differential scanning calorimetry. The PET crystallization rate increases significantly with increasing silica content, which indicates that the silica nanoparticles act as an efficient nucleating agent to facilitate PET crystallization. Using Avrami analysis, for the first time, preferred 1-D crystal growth was confirmed for geometrically confined nanocomposite fibers. Addition of silica particles makes the crystal growth more likely to occur in a 1-D manner.

Keywords Thermal analysis · Electrospinning · Nanocomposite · Reinforcement

Introduction

Poly(ethylene terephthalate) (PET) composites with nano-size inorganic reinforcement are of great interest due to the improvement in electrical, mechanical, and thermal properties as well as high performance in fire retardance, solvent and heat resistance, wettability, and dyeability compared to neat PET [1–8]. Among the diverse traditional reinforcements doped in PET, such as carbon nanotubes [9], nanoclays [10], and gold nano-wires [11], the influence of silica on the nucleation and crystallization behaviors of PET has received considerable attention [12, 13]. Experimental results show that in non-isothermal crystallization, silica particles in contact with the PET matrix can induce a heterogeneous nucleation effect, producing branched and crosslinked macromolecules [13]. Meanwhile, the nucleation rate induced by silica particles was increased with a decrease in particle size; 35 nm silica particles produced the most significant effect [12].

Electrospinning (ES) has been widely investigated and proved to be an effective way to prepare high performance nanocomposite fibers. By adopting appropriate surface modification of inorganic fillers, solution properties, and processing conditions, electrospun fibers with highly regular diameters and smooth surfaces could be obtained. A series of studies has been carried out in our group to characterize the morphology, thermal transitions, and phase structures of electrospun nanocomposite fiber [9, 14, 15]. Previous study based on the specific reversing heat capacity of PET/silica, electrospun nanocomposite fibers [15] demonstrated the existence of the rigid amorphous phase in the absence of PET crystallinity. Experimental results show that the rigid amorphous fraction (RAF) can be formed by interaction with either or both the silica particles and the lamellar crystals, and these two origins of confinement coexist in the crystallized fiber. Thermal analysis of nanocomposites is a powerful tool to characterize phase structure in nanocomposite fiber, and is especially useful to quantify the immobilized rigid amorphous phase around fillers.

In this paper, for the first time, the nucleating effect of silica on PET nanocomposite fibers during isothermal crystallization was characterized. The influence of silica

Q. Ma · B. Mao · P. Cebe (✉)
Department of Physics and Astronomy, Center for Nanoscopic Physics, Tufts University, Medford, MA 02155, USA
e-mail: peggy.cebe@tufts.edu

particles on the phase structure of both as-spun amorphous and isothermally crystallized nanocomposite fibers was also examined using both differential scanning calorimetry (DSC) and Fourier transform infrared spectroscopy (FTIR). Systematic investigation through thermal analysis of the crystal nucleation and chain confinement of PET brought by silica particle reinforcement enables a deeper understanding of the specific properties of PET-based nanocomposites.

Experimental section

Materials

PET was obtained from the former Allied Signal Corp. as film, with intrinsic viscosity of 0.92 dL g^{-1}, measured in 60/40 phenol/trichloroethylene solution. The molecular weight is 25,000 g mol^{-1} calculated from the Mark-Houwink equation with $a = 0.640$ and $K = 14 \times 10^{-4}$ dL g^{-1}. Silicon dioxide nanopowder was purchased from Aldrich, with a particle diameter of 16 nm. Surface modification of neat silica was carried out using methyltrichlorosilane. Methyltrichlorosilane was added to toluene at a volume-to-volume ratio of 10 %. Then silica powder was added into the methyltrichlorosilane/toluene solution at a loading of 5 wt% in the total mixed solvent. The solution was stirred overnight at room temperature. Then, the majority of the solvent was evaporated from the silica under ambient conditions and further eliminated in a vacuum oven at 100 °C for 12 h. The resulting silane-modified SiO_2 powders were dispersed in hexafluoro-isopropanol (HFIP) to form the silica stock solution and ultrasonicated 24 h to minimize possible agglomerates. To prepare the polymer solutions, PET pellets were dissolved in HFIP solvent at a concentration of 15 wt% PET and ultrasonicated overnight. Then PET/SiO_2 solutions were mixed together to obtain the following specific weight ratios of SiO_2 to PET: 0, 0.5, 1.0, and 2.0 wt%, and the mixed solution was electrospun.

ES process

PET/silica solution was loaded into an inclined 0.55-mm inner diameter pipette with a copper needle electrode inside, at a working distance of 15 cm from a grounded collector covered with Al foil. A high voltage of 15 kV was applied to provide the required electrical field. The as-spun fibers deposited on the collector were then immersed in methanol for 2 h to remove any residual HFIP and then dried in a vacuum oven for 24 h at room temperature.

Differential scanning calorimetry (DSC)

A TA Instruments Q100 temperature modulated DSC (TMDSC) was used to perform the thermal analysis experiments. Calibration with indium was conducted for the heat flow and temperature, and the experimental heat capacity was evaluated using a sapphire standard. The flow rate for using nitrogen as the purge gas is 50 mL min^{-1}. The sample mass was kept around 6 mg. The Al sample and reference pans were identical in mass with an error ± 0.01 mg.

The heat capacity in this paper was obtained using the three-run method. The first run is empty Al sample pan versus empty Al reference pan to obtain baseline correction. The second run is sapphire standard versus empty Al reference pan to calibrate heat flow amplitude. The third run is sample versus empty reference pan. The heat capacity was calculated from the heat flow contribution of the polymer part only (i.e., the heat flow obtained in the third run was corrected by subtracting the contribution of silica particles during heating.)

Scanning electron microscopy (SEM)

An FESEM Ultra 55 SEM was used to examine the morphology of electrospun fibers at Harvard University, Center for Nanoscale Systems. Samples were sputter-coated with gold–palladium before viewing.

Atomic force microscopy (AFM)

Fiber imaging was carried out using Nanoscope V, Dimension 3100 AFM (Digital Instruments, Santa Barbara, CA). For AFM, PET/silica ES fibers were cast onto a silicon wafer to form a thin mat for analysis. FESP silicon probes were used to investigate the fiber with resonance frequency of 75 kHz and force constant of 2.8 N m^{-1} as specified by the manufacture.

Fourier Transform Infrared Spectroscopy (FTIR)

FTIR absorbance spectra was collected using a JASCO 6200 spectrometer in attenuated total reflection (ATR) mode. Sixty-four scans were co-added with a resolution of 4 cm^{-1} in the wave number region of 600–4,000 cm^{-1} for one single sample test.

Results and discussion

Morphology of nanocomposite fibers

SEM was used to investigate the morphology of PET/silica electrospun nanocomposite fiber. For the sake of brevity, only the image of PET with 2 % silica is shown in Fig. 1. Uniform and smooth electrospun fibers were obtained from both PET homopolymer and nanocomposite solutions, indicating the good dispersion of silica in PET matrix.

AFM imaging was performed under ambient conditions in tapping mode using FESP cantilevers with scan rate 0.5 Hz. Figure 2a shows the topography image of a single electrospun fiber with 200-nm diameter. The cross-section of the topography of the sample (Fig. 2b), taken along the line marked by the arrows in Fig. 2a, shows a smooth round top of the fiber. The height of the fiber is a reliable measure of the fiber diameter ($\sim$185 nm) while the width of the fiber in the image is exaggerated due to the convolution of the AFM tip shape with the shape of the fiber [16].

Phase structure of as-spun fibers

Previous study in our group [15] showed that the PET/Silica as-spun fiber is non-crystalline based on the absence of crystalline reflections from wide angle X-ray scattering (WAXS). The existence of RAF in non-crystallized as-spun PET/Silica nanocomposite fibers was quantitatively demonstrated based on the reduction of heat capacity step at T_g compared with fully amorphous unconstrained PET [15]. The method used to determine the immobilized fraction is explained in the sketch of Fig. 3, which shows the specific reversing heat capacity trace of amorphous PET (solid curve) in comparison to PET with 2 % silica nanocomposite fiber (dashed curve). If no confinement exists in as-spun fiber and the polymer chains possess full mobility, the heat capacity will match the 100 % liquid baseline above T_g (e.g., solid curve); however, if confinement of any origin exists, there will be a significant reduction in heat capacity step at T_g (e.g., dashed curve), and this confinement can only be attributed to the formation of a rigid immobilized layer around silica particles in the as-spun amorphous fibers.

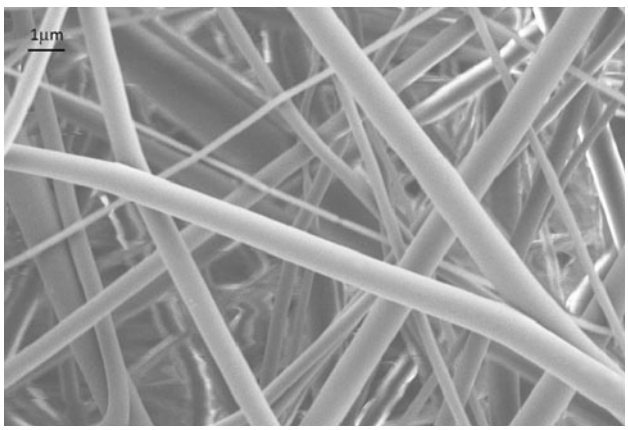

Fig. 1 SEM image of as-spun PET nanofibers with 2.0 % silica. Scale bar is 1 micron

The existence of an immobilized RAF layer was also verified by FTIR spectroscopy of as-spun PET/silica fibers. Figure 4a shows FTIR absorbance of the untreated, as-spun ES fibers. The absorption peak at 1,174 cm^{-1} is assigned to the phenyl ring vibration associated with mobile amorphous regions of PET while the 1,410 cm^{-1} serves as a reference band [18, 19]. As the silica loading increased, the absorption peak at 1,174 cm^{-1} was suppressed until reaching a minimum value for the sample of PET with 2 % silica, indicating a decrease in the mobile amorphous fraction. Based on previous study of WAXS, no crystallinity was found in the as-spun fibers, so we attribute the reduction in phenyl ring absorbance to the emergence of the rigid amorphous phase. Normalizing intensity of the 1,174 cm^{-1} band to the reference band, ϕ_{RAF} is

$$\phi_{RAF} = 1 - (A^{sc}/A^{0}) \quad (1)$$

where A^{sc} is the intensity ratio of the absorption peak at 1,174 cm^{-1} to that at 1,410 cm^{-1} for all semicrystalline nanocomposite samples, and A^{0} is the intensity ratio of the absorption peak at 1,174 cm^{-1} to that at 1,410 cm^{-1} for neat PET homopolymer fiber. Figure 4b shows the comparison of ϕ_{RAF} from FTIR and DSC. We see that the FTIR results have the same growth trend as the previous thermal analysis results.

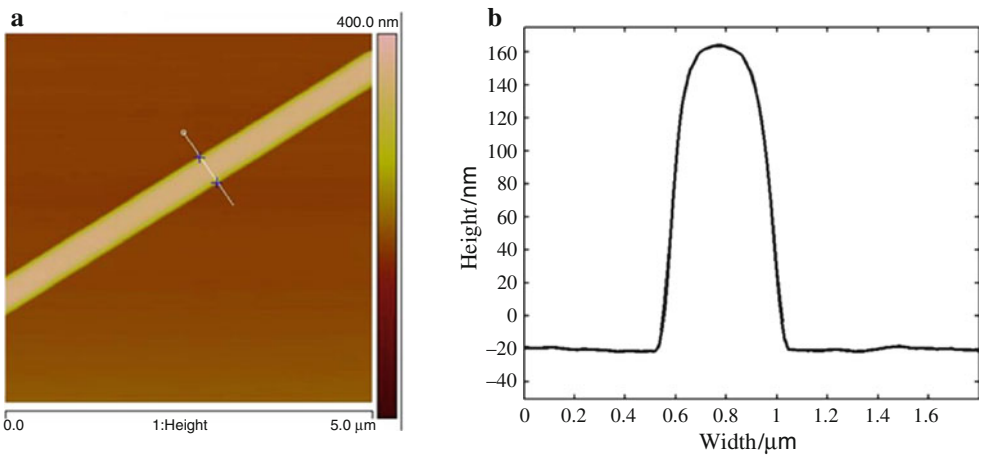

Fig. 2 **a** AFM topography image of a single electrospun PET fiber with 1.0 % modified silica; **b** Height profile across the section of the fiber taken at the position marked by the arrows in (**a**)

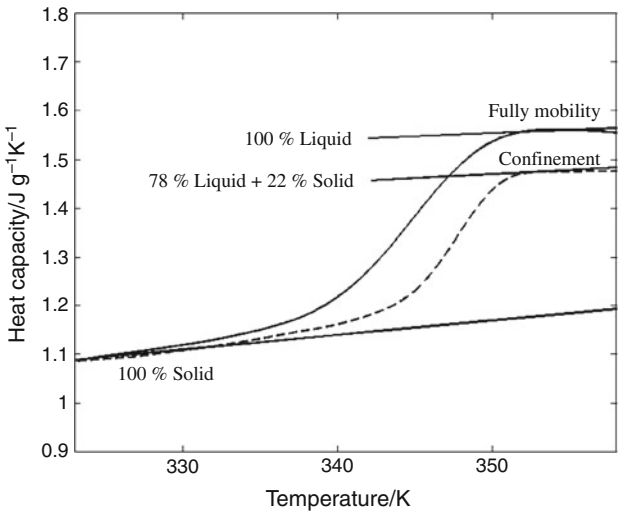

Fig. 3 Sketch showing the method of determining heat capacity increment at T_g from a plot of the specific reversing heat capacity versus temperature. *Solid* and *dashed curves* stand for heat capacity of PET homopolymer and PET/2 % silica nanocomposite fibers, respectively. The line of 100 % solid and 100 % liquid were drawn based on data from ATHAS databank [17]. The middle line represents the heat capacity calculated based on the 78 % liquid fraction plus 22 % solid fraction

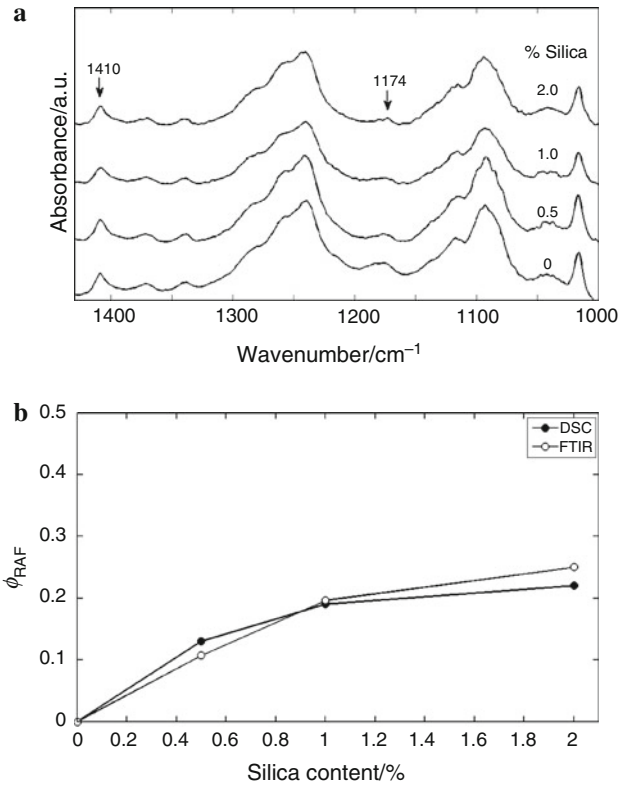

Fig. 4 **a** FTIR absorbance versus wavenumber for amorphous, as-spun PET nanofibers containing modified silica, at the weight percentages listed. *Arrows* mark the phenyl ring vibration at 1,174 cm^{-1} and the reference band at 1,410 cm^{-1}; **b** Comparison of ϕ_{RAF} obtained from FTIR (*open circles*) and DSC (*filled circles*)

DSC studies of isothermal crystallization

The addition of silica nanoparticles can not only cause a restriction to the polymer chain mobility by inducing an immobilized layer, but also has been demonstrated to have a significant effect on the crystallization kinetics through changing crystal nucleation and growth. It has been widely demonstrated that the crystallization behavior of PET can be influenced or controlled by inorganic silica particles [8, 12, 13, 20–22]. A series of experiments was carried out to study the effect of silica particles on the isothermal cold crystallization (i.e., crystallization of the fibers conducted by heating the fibers above the glass transition temperature, $T_g = 345$ K) of PET electrospun fibers. Isothermal cold crystallization kinetics for PET/Silica nanofiber was investigated using standard DSC to evaluate the effect of SiO_2 nanoparticles on crystallization rate of PET fibers. All samples were heated very rapidly to the specific crystallization temperature $T_c = 375$ K and isothermally crystallized at T_c for various times. The exothermic heat flow rate $dH(t)/dt$, as a function of time, t, at T_c is shown in Fig. 5. The asymmetric shapes of the exothermal peaks suggest that this process contains secondary crystallization in the later state of crystal growth [23]. Crystallization time was extended until no more exothermic heat flow could be detected.

The relative crystallinity is obtained from the integrated normalized heat flow rate as a function of time, which is written as [23–25]:

$$X_C = H(t)/H(\infty) = \left[\int_0^t \mathrm{d}t(\mathrm{d}H(t)/\mathrm{d}t)\right] \Big/ \left[\int_0^\infty \mathrm{d}t(\mathrm{d}H(t)/\mathrm{d}t)\right] \quad (2)$$

where X_C is the ratio of heat generated at time t, $H(t)$, to the entire heat generated during crystallization, $H(\infty)$, and is shown in Fig. 6.

The Avrami equation [26–28] is adopted to analyze the crystallization kinetics of PET/Silica nanocomposite fibers:

$$X_c(t) = 1 - \exp(-Kt^n) \quad (3)$$

where $X_c(t)$ is the relative crystallinity of samples at different times, K is the crystallization rate coefficient, which is a function of temperature and relates to both the nucleation frequency and the crystal growth rate, and n is the Avrami exponent parameter which reflects the nucleation mechanism and crystal growth geometry [29]. Figure 7 shows the double-logarithmic Avrami plot for PET fibers with different amounts of modified silica. K and n, summarized in Table 1, are constants with values specific to a given crystalline morphology and type of nucleation for a particular crystallization condition, and are determined

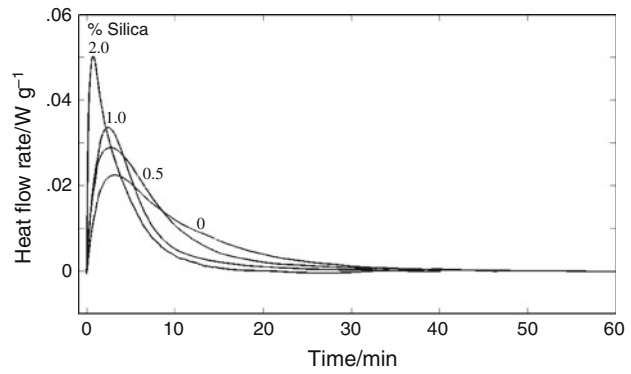

Fig. 5 Isothermal crystallization kinetics at 375 K of PET/silica fibers investigated by standard DSC. The exothermic heat flow rate, d$H(t)$/dt, versus time, t, is shown for PET with different amount of silica. Wt% of silica is indicated

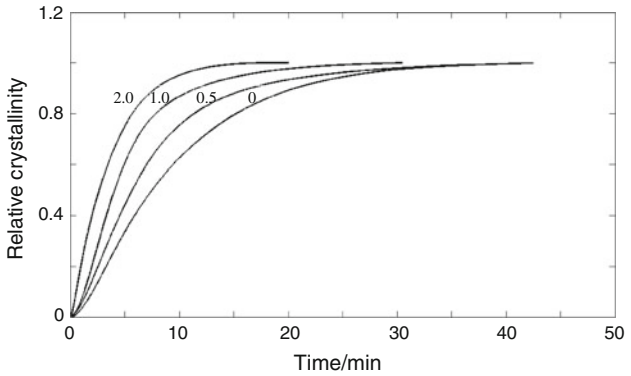

Fig. 6 Relative crystallinity versus crystallization time for PET/silica fibers crystallized at 375 K, calculated from Eq. (2). Wt% of silica is indicated

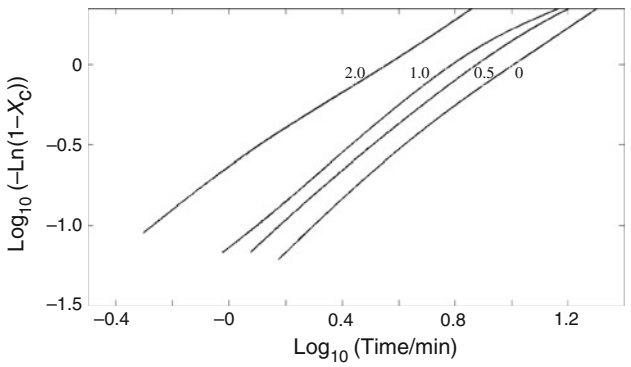

Fig. 7 Avrami plot of the isothermal crystallization kinetics of PET/silica fibers crystallized at 375 K. Wt% of silica is indicated

from the intercept and slope of the linear portion (before the roll off due to secondary crystallization) of the plot of $\log[-\ln(1 - X_c)]$ versus $\log(t)$.

Two characteristic times are also listed in Table 1: the calculated crystallization halftime, $t_{1/2}^{cal}$, and the time to maximum rate of change of crystallinity, t_i. Calculated halftime is the time when the relative crystallinity has reached 0.5, obtained from [24]

$$t_{1/2}^{cal} = ((\ln 2)/K)^{1/n} \quad (4)$$

The experimentally determined crystallization halftime derived from Fig. 6, $t_{1/2}^{exp}$, is also given for comparison in Table 1. The time to maximum rate of heat flow, t_i, can be deduced from n and K as described below in Eq. (5), and is included in Table 1 for comparison to the halftimes:

$$t_i = ((n-1)/nK)^{1/n} \quad (5)$$

For all samples, the Avrami exponent, n, maintains a value between 1.15 and 1.31, indicating preferred 1-D crystal growth in PET fiber, compared to cold crystallization of pure PET film which follows 3-D spherical growth with heterogeneous nuclei [30]. ES of nanoscale fibers results in a geometrical size restriction, and polymer chains become stretched and confined along the fiber axis. This induces linear growth of crystals within the fiber. Existing silica particles may serve as nuclei, and the stretched chains could be absorbed onto the edge and/or surface of these nuclei and then grow outward [31]. As a result, n values approach unity as the silica amount increases, making the crystal more likely to grow in a linear manner. Small angle X-ray studies are underway to determine the directionality of the one-dimensional growth.

The crystallization rate coefficient, K, decreases with the loading amount of silica particles. A marked decrease in the induction time t_i with silica amount could be observed. $t_{1/2}$ is always larger than t_i, and the difference between the two times decreases with an increase of silica, indicating the asymmetry is getting less pronounced when the inorganic particle content increases.

From Fig. 6, the degree of crystallization conversion versus time curves show that for all the samples loaded with silica, the time needed in order for the crystallization process to be completed is decreased, compared to that of neat PET. The PET crystallization rate increases significantly with an increase of the silica content, which indicates that the silica nanoparticles act as an efficient nucleating agent to facilitate PET crystallization. The addition of silica could decrease the activation energy compared to neat PET, so once crystals are nucleated, silica particles could largely accelerate the crystal growth rate [13, 32].

After crystallization, all samples were heated to the melt at a heating rate of 5 K min^{-1}. The phase structures were evaluated using a three-run method described in earlier work [14], and the results are shown in Table 2. Compared to neat PET ES fiber, PET/silica nanocomposite ES fibers possess a similar degree of crystallinity, but an increase of RAF occurs with an increase of the silica loading. Here,

Table 1 Parameters characterizing isothermal crystallization at 375 K of PET/silica electrospun nanofibers: Avrami rate constant, K, and exponent, n, calculated and experimental crystallization halftimes, and time to maximum rate of change of crystallinity

Sample	log K (±0.05)	n (±0.05)	$t_{1/2}^{cal}$/min (±0.1)	$t_{1/2}^{exp}$/min (±0.1)	t_i/min (±0.1)
PET	−1.33	1.31	7.81	7.73	3.44
PET/0.5 % silica	−1.17	1.30	6.00	5.91	2.57
PET/1.0 % silica	−1.03	1.25	4.96	5.08	1.94
PET/2.0 % silica	−0.64	1.15	2.62	2.60	0.61

Table 2 Phase structure of PET/silica ES nanofibers isothermally cold crystallized at 375 K: crystal, mobile amorphous and rigid amorphous fractions

Sample	ϕ_C (±0.01)	ϕ_{MAF} (±0.01)	ϕ_{RAF} (±0.02)
PET	0.32	0.32	0.36
PET/0.5 % silica	0.31	0.29	0.40
PET/1.0 % silica	0.30	0.28	0.42
PET/2.0 % silica	0.30	0.25	0.45

RAF includes both the immobilized layer around silica particles and the interface between crystalline and mobile amorphous chains.

Conclusions

PET/silica fibers of high quality were fabricated from ES. Using FTIR, the existence of the immobilized layer induced by the reinforcement was further verified in the as-spun amorphous fiber, consistent with previous thermal analysis results. The addition of silica particles not only introduces polymer-filler interfacial binding, leading to the immobilized layer, but also has a significant effect on the crystallization kinetics of nanocomposite fibers. For the first time, the preferred 1-D crystal growth was confirmed for the geometrically confined nanocomposite fiber. The addition of silica particles makes the crystal growth more likely to occur in a 1-D manner.

Acknowledgements The authors thank the National Science Foundation, Polymers Program of the Division of Materials Research for support of this research under DMR-0602473 and the NSF MRI Program under DMR-0520655 which provided thermal analysis instrumentation. Portions of this research were conducted at Harvard University's Center for Nanoscale Systems.

References

1. Chung JW, Son SB, Chun SW, Kang TJ, Kwak SY. Thermally stable exfoliated poly(ethylene terephthalate) (PET) nanocomposites as prepared by selective removal of organic modifiers of layered silicate. Polym Degrad Stabil. 2008;93:252.
2. Guan G, Li C, Yuan X, Xiao Y, Liu X, Zhang D. New insight into the crystallization behavior of poly(ethylene terephthalate)/clay nanocomposites. J Polym Sci Polym Phys. 2008;46:2380.
3. Hwang SY, Lee WD, Lim JS, Park KH, Im SS. Dispersibility of clay and crystallization kinetics for in situ polymerized PET/pristine and modified montmorillonite nanocomposites. J Polym Sci Polym Phys. 2008;46:1022.
4. Ammala A, Bell C, Dean K. Poly(ethylene terephthalate) clay nanocomposites: improved dispersion based on an aqueous ionomer. Compos Sci Technol. 2008;68:1328.
5. Chung SC, Hahm WG, Im SS, Oh SG. Poly(ethylene terephthalate)(PET) nanocomposites filled with fumed silicas by melt compounding. Macromol Res. 2002;10:221.
6. Xu X, Ding Y, Qian Z, Wang F, Wen B, Zhou H, Zhang S, Yang M. Degradation of poly(ethylene terephthalate)/clay nanocomposites during melt extrusion: Effect of clay catalysis and chain extension. Polym Degrad Stabil. 2009;94:113.
7. Liu W, Tian X, Cui P, Li Y, Zhang K, Yang Y. Preparation and characterization of PET/silica nanocomposites. J Appl Polym Sci. 2004;91:1229.
8. Bikiaris D, Karavelidis V, Karayannidis G. A new approach to prepare poly(ethylene terephthalate)/silica nanocomposites with increased molecular weight and fully adjustable branching or crosslinking by SSP. Macromol Rapid Commun. 2006;27:1199.
9. Chen H, Liu Z, Cebe P. Chain confinement in electrospun nanofibers of PET with carbon nanotubes. Polymer. 2009;50:872.
10. Ke Y, Long C, Qi Z. Crystallization, properties, and crystal and nanoscale morphology of PET-clay nanocomposites. J Appl Polym Sci. 1999;71:1139.
11. Siegel J, Slepička P, Heitz J, Kolská Z, Sajdl P, Švorčík V. Gold nano-wires and nano-layers at laser-induced nano-ripples on PET. Appl Surf Sci. 2010;256:2205.
12. Ke YC, Wu TB, Xia YF. The nucleation, crystallization and dispersion behavior of PET-monodisperse SiO_2 composites. Polymer. 2007;48:3324.
13. Antoniadis G, Paraskevopoulos KM, Bikiaris D, Chrissafis K. Non-isothermal crystallization kinetic of poly(ethylene terephthalate)/fumed silica (PET/SiO(2)) prepared by in situ polymerization. Thermochim Acta. 2010;510:103.
14. Ma Q, Cebe P. Phase structure of electrospun poly(trimethylene terephthalate) composite nanofibers containing carbon nanotubes. J Therm Anal Calorim. 2010;102:425.
15. Ma Q, Mao B, Cebe P. Chain confinement in electrospun nanocomposites: using thermal analysis to investigate polymer-filler interactions. Polymer. 2011;52:3190.
16. Kim JS, Reneker DH. Polybenzimidazole nanofiber produced by electrospinning. Polym Eng Sci. 1999;39:849.
17. Pyda M. ATHAS data bank, http://athas.prz.rzeszow.pl/, 2008.
18. Cole KC, Ajji A, Pellerin E. New insights into the development of ordered structure in poly(ethylene terephthalate). 1. Results from external reflection infrared spectroscopy. Macromolecules. 2002;35:770.

19. Stokr J, Schneider B, Doskocilova D, Lovy J, Sedlacek P. Conformational structure of poly(ethylene terephthalate). Infra-red, Raman and n.m.r. spectra. Polymer. 1982;23:714.
20. Yang Y, Xu H, Gu H. Preparation and crystallization of poly(ethylene terephthalate)/SiO_2 nanocomposites by in situ polymerization. J Appl Polym Sci. 2006;102:655.
21. Wang Y, Shen C, Li H, Li Q, Chen J. Nonisothermal melt crystallization kinetics of poly(ethylene terephthalate)/clay nanocomposites. J Appl Polym Sci. 2004;91:308.
22. He JP, Li HM, Wang XY, Gao Y. In situ preparation of poly(ethylene terephthalate)-SiO_2 nanocomposites. Eur Polym J. 2006;42:1128.
23. Hu X, Lu Q, Kaplan D, Cebe P. Microphase separation controlled beta-sheet crystallization kinetics in fibrous proteins. Macromolecules. 2009;42:2079.
24. Xu JT, Fairclough JPA, Mai SM, Ryan AJ, Chaibundit C. Isothermal crystallization kinetics and melting behavior of poly(oxyethylene)-b-poly(oxybutylene)/poly(oxybutylene). Macromolecules. 2002;35:6937.
25. Choi J, Kwak SY. Architectural effects of poly(epsilon-caprolactone)s on the crystallization kinetics. Macromolecules. 2004; 37:3745.
26. Avrami M. Kinetics of phase change I: general theory. J Chem Phys. 1939;7:1103.
27. Avrami M. Kinetics of phase change. II Transformation-time relations for random distribution of nuclei. J Chem Phys. 1940; 8:212.
28. Avrami M. Granulation, phase change, and microstructure: kinetics of phase change. III. J Chem Phys. 1941;9:177.
29. Wunderlich B. Marcromolecular physics, vol 2, crystal nucleation, growth, annealing. New York: Academic Press; 1976.
30. Lu XF, Hay JN. Isothermal crystallization kinetics and melting behaviour of poly(ethylene terephthalate). Polymer. 2001;42:9423.
31. Tan S, Su A, Li W, Zhou E. New insight into melting and crystallization behavior in semicrystalline poly(ethylene terephthalate). J Polym Sci Polym Phys. 2000;38:53.
32. Turturro G, Brown GR, St-Pierre LE. Effect of silica nucleants on the rates of crystallization of poly (ethylene terephthalate). Polymer. 1984;25:659.